Am J Physiol Cell Physiol 319: C218–C232, 2020.
First published May 20, 2020; doi:10.1152/ajpcell.00153.2020.

RESEARCH ARTICLE

Mechanisms of altered skeletal muscle action potentials in the R6/2 mouse model of Huntington's disease

Daniel R. Miranda,[1] Eric Reed,[1] Abdulrahman Jama,[2] Michael Bottomley,[3] Hongmei Ren,[2] Mark M. Rich,[4] and Andrew A. Voss[1]

[1]*Department of Biological Sciences, Wright State University, Dayton, Ohio;* [2]*Department of Biochemistry and Molecular Biology, Wright State University, Dayton, Ohio;* [3]*Department of Mathematics and Statistics, Wright State University, Dayton, Ohio; and* [4]*Department of Neuroscience, Cell Biology, and Physiology, Wright State University, Dayton, Ohio*

Submitted 16 April 2020; accepted in final form 15 May 2020

Miranda DR, Reed E, Jama A, Bottomley M, Ren H, Rich MM, Voss AA. Mechanisms of altered skeletal muscle action potentials in the R6/2 mouse model of Huntington's disease. *Am J Physiol Cell Physiol* 319: C218–C232, 2020. First published May 20, 2020; doi:10.1152/ajpcell.00153.2020.—Huntington's disease (HD) patients suffer from progressive and debilitating motor dysfunction for which only palliative treatment is currently available. Previously, we discovered reduced skeletal muscle Cl^- channel (ClC-1) and inwardly rectifying K^+ channel (Kir) currents in R6/2 HD transgenic mice. To further investigate the role of ClC-1 and Kir currents in HD skeletal muscle pathology, we measured the effect of reduced ClC-1 and Kir currents on action potential (AP) repetitive firing in R6/2 mice using a two-electrode current clamp. We found that R6/2 APs had a significantly lower peak amplitude, depolarized maximum repolarization, and prolonged decay time compared with wild type (WT). Of these differences, only the maximum repolarization was accounted for by the reduction in ClC-1 and Kir currents, indicating the presence of additional ion channel defects. We found that both $K_V1.5$ and $K_V3.4$ mRNA levels were significantly reduced in R6/2 skeletal muscle compared with WT, which explains the prolonged decay time of R6/2 APs. Overall, we found that APs in WT and R6/2 muscle significantly and progressively change during activity to maintain peak amplitude despite buildup of Na^+ channel inactivation. Even with this resilience, the persistently reduced peak amplitude of R6/2 APs is expected to result in earlier fatigue and may help explain the motor impersistence experienced by HD patients. This work lays the foundation to link electrical changes to force generation defects in R6/2 HD mice and to examine the regulatory events controlling APs in WT muscle.

action potential; chloride channel; Huntington's disease; potassium channel; skeletal muscle

INTRODUCTION

Huntington's disease (HD) is a monogenic disorder caused by a trinucleotide (CAG) repeat expansion in the huntingtin (*HTT*) gene. Mutant *HTT* is expressed ubiquitously and leads to central and peripheral pathology (41, 55, 61). The motor symptoms of Huntington's disease include involuntary muscle contractions that can lead to chorea (irregular jerky movements), bradykinesia (slow movement), dystonia (abnormal positioning), and muscle rigidity. HD patients also suffer from reduced lower limb muscle strength (10), which may contribute to impairments in balance and mobility (14).

Correspondence: A. A. Voss (andrew.voss@wright.edu).

We previously discovered a decrease in skeletal muscle Cl^- channel (ClC-1) and inwardly rectifying K^+ channel (Kir) currents, as well as aberrant splicing of the gene encoding ClC-1, *Clcn1*, in the R6/2 transgenic mouse model for Huntington's disease (68). Moreover, we found that the reduction in ClC-1 currents and *Clcn1* aberrant splicing progressed over the same time course as the disease, suggesting that ClC-1 defects contribute to the overall R6/2 mouse pathology (44). ClC-1 and Kir currents act to maintain the resting membrane potential in skeletal muscle. To drive the membrane potential to threshold and trigger an action potential (AP), excitatory currents need to overcome the ClC-1 and Kir currents (27, 31, 32, 56, 57). Consistent with this role for ClC-1 and Kir currents, we showed that significantly less current was needed to trigger an AP in R6/2 compared with wild-type fibers (67). Thus, the R6/2 skeletal muscle was hyperexcitable. The effects of the reduced R6/2 ClC-1 and Kir currents on AP properties, particularly during trains, as would occur during muscle activity, is not known. A likely mechanism by which reduced ClC-1 and Kir currents affect R6/2 pathology is by prolonging muscle APs during repetitive stimulation. At high frequencies of stimulation, the prolonged repolarization is expected to increase inactivation of the fast voltage-gated Na^+ channels ($Na_V1.4$). A substantial inactivation of $Na_V1.4$ should result in AP failure or degradation and the eventual loss of muscle excitability that would present as muscle fatigue (69).

The objective of this study was to determine the effect of the reduced ClC-1 and Kir currents on APs as well as to identify any additional ion channel defects that affect single or repetitive APs. Beyond revealing the effect of reduced ion channel activity on R6/2 muscle APs, this study provides one of the most complete examinations of the dynamic properties of WT APs during repetitive stimulation. Our work demonstrates an important role of Cl^- movement during normal repetitive activity in wild-type muscle as well as a striking capacity of WT and disease muscle to maintain AP firing throughout periods of considerable $Na_V1.4$ inhibition.

MATERIALS AND METHODS

Ethical Approval

All animal procedures were performed with the approval of the Animal Care and Use Committee of Wright State University. We established a breeding colony in the Wright State University Laboratory Animal Resources Facility that consisted of one wild-type (WT)

B6CBA female with an ovarian transplant [hemizygous for Tg(HDexon1)62Gpb] and one WT male (B6CBAF1/J) purchased from The Jackson Laboratory, stock no. 002810 (RRID: IMSR_JAX: 002810). A total of six male and four female R6/2 mice, as well as five male and five female WT mice produced from seven breeding pairs, were used for this study. Tail samples cut between 7 and 14 days of age were genotyped at Laragen, Inc. (Culver City, CA). Mice were housed with WT littermates (control) in sex-matched cages after weaning at ~14 days of age. Environmental conditions were maintained with a 12-h light-dark cycle and constant temperature (21–23°C) and humidity (55 ± 10%). The cages contained corncob bedding (Harlan Teklad 7902) and environmental enrichment (mouse house and cotton nestlet). Mice were supplied with dry chow (irradiated rodent diet; Harlan Teklad 2981) and water ad libitum. Beginning at 10 wk of age, all cages housing R6/2 mice were supplied with a petri dish containing moist chow (dry chow soaked in water) to ensure adequate nutritional intake in the symptomatic mice. For the 9-AC/Ba^{2+} group, WT, noncarrier [B6CBA-Tg(HDexon1)62Gpb/1J wild-type mice] mice from The Jackson Laboratory (stock no. 100011; RRID:IMSR_JAX:100011) were used and housed under the same conditions as the R6/2 mice. A total of three female WT mice produced from one breeding pair were used for the 9-AC/Ba^{2+} group.

Behavioral Assessment

The health and phenotype severity assessments for HD mice, as described previously (44, 68), were performed weekly for mice 8–10 wk of age, every other day for mice 10 wk of age, and daily for mice ≥11 wk of age. Assessment categories included physical condition, activity level, and weight loss. Of the behavioral measures, mouse weight has been a reliable and easy way to obtain measurement to assess disease progression. We previously showed that R6/2 weight stopped increasing from 6 to 10 wk of age and decreased after 10 wk of age (44).

Electrophysiology

Mice were euthanized by inhalation of a saturating dose of isoflurane (~2 g/L), followed by cervical dislocation. All R6/2 and control mice were between 11 and 13 wk of age. Hindlimb flexor digitorum brevis and interosseous muscles were dissected and enzymatically dissociated at 35–36°C under mild agitation for ~1 h using 1,000 U/mL of collagenase type IV (Worthington Biochemical). Collagenase was dissolved in an extracellular solution (see below). Dissociation was completed using mild trituration in extracellular solution with no collagenase. The fibers were allowed to recover at 21–23°C for 1 h before electrical measurements were recorded. The flexor digitorum brevis and interosseous muscle groups were chosen because they can both be easily dissected from the mouse paws and are composed of small fibers (400–500 μm in length) that primarily express the fast type II myosin heavy chain (8, 22, 24, 44). Fibers from both muscle groups were pooled for electrophysiology experiments.

Fibers were visualized with an Olympus BX51WI or IX71 microscope. The BX51WI microscope was equipped with ×10 (UMPLFLN10XW) and ×40 (LUMPLFLN40XW) objectives, and the IX71 microscope was equipped with ×10 (UPlanFLN) and ×20 (UPlanFLN) objectives. Electrical properties were measured under standard current clamp conditions at 21–23°C using two borosilicate intracellular microelectrodes with a 1.5-mm outside diameter and 0.86-mm inside diameter (Sutter Instruments), an Axoclamp 900A amplifier, a Digidata 1550 digitizer, and pCLAMP 10 or 11 data acquisition and analysis software (Molecular Devices). The Axoclamp 900A was equipped with a virtual-ground headstage (VG-9Ax100). Reference electrodes were placed in separate cups containing 3 M KCl and connected to the extracellular fluid via agar bridges. Electrodes were impaled ~10 μm apart from each other. The voltage-sensing electrode was connected with an Axoclamp HSx1 headstage, and the current-passing electrode was connected with an Axoclamp HSx10 headstage that was modified to have a 2 MΩ output resistor (HSx5). Both the current-passing and voltage-sensing electrodes were filled with the same internal solution (below). Electrode resistances for each electrode were between 10 and 15 MΩ. Data were acquired at 100 kHz. Current and voltage records were low-pass filtered with the internal Axoclamp 900A filters at 6 kHz.

Upon impalement of each fiber, the intracellular solution was allowed to equilibrate with the sarcoplasm for 20 min, and the baseline membrane potential was maintained at approximately –85 mV by injecting a constant negative current. Fibers that exceeded –20 nA of holding current, which indicated membrane damage, were excluded from the study. Action potentials (APs) were elicited by 0.2-ms current pulses with an amplitude equal to 1.1× the threshold for firing an AP. A single AP was triggered 75 ms before each train to use as a reference. Trains of APs, 5 s in duration and of increasing frequency (from 20 to 40 to 60 Hz) were measured from each fiber, with ≥1 min between each train. If a fiber did not fully repolarize within 1 min after each train, the holding current was adjusted to bring the membrane potential back to –85 mV. To examine recovery, 7 APs at 0.5 Hz were recorded after each train. To prevent contractions, 70 mM EGTA was added to the intracellular solution.

Intracellular and Extracellular Buffers for Electrophysiology

Extracellular solution (in mM) was as follows: 139 NaCl, 4 KCl, 5 $CaCl_2$, 2 $MgCl_2$, 5 glucose, 1 NaH_2PO_4, and 10 MOPS, pH 7.4 (NaOH); 0.03 9-anthracene carboxylic acid (9-AC) and 0.00073 $BaCl_2$ were added when partially blocking ClC-1 and Kir, respectively.

Intracellular solution (in mM) was as follows: 5 $MgCl_2$, 5 ATP disodium, 5 phosphocreatine disodium, 5 glutathione, 40 MOPS, and 70 EGTA, pH 7.2 (KOH).

Chemicals

Chemicals were purchased from Fisher Scientific; exceptions include $CaCl_2$ and $MgCl_2$ stock solutions (TekNova), ATP di-Na (Sigma-Aldrich), $BaCl_2$ (Matheson, Colman and Bell), and anthracene-9-carboxylic acid (Tocris).

RNA Extraction and Real-Time PCR

Total RNA was isolated from the interosseous of 11 to 12 wk old R6/2 mice and their age-matched WT littermates using TRIzol reagent (Thermo Fisher Scientific; no. 15596018) according to the manufacturer's instructions. One microgram of total RNA was used for reverse transcription with the High-Capacity cDNA Reverse Transcription Kit (no. 4368814; Thermo Fisher Scientific). The real-time PCR reaction was carried out in a QuantStudio Real-Time PCR System (Thermo Fisher Scientific) using SYBR Green Real-time PCR Master Mix (no. A25742; Thermo Fisher Scientific). Expression data were normalized to the housekeeping gene *β-actin* and the relative mRNA expression was determined by the comparative Ct ($2^{-\Delta\Delta Ct}$). PCR was performed using primers for K_V3.4 (forward: 5′-TGG GCT GTG GTC ACC ATG AC-3′; reverse: 5′-CTC TCG ACC ACA CCC TCT TCC-3′), K_V1.5 (forward: 5′-TCCGACG-GCTGGACTCAATAA-3′; reverse: 5′-CAGATGGCCTTCTAG-GCTGTG-3′), and Kv1.4 (F1: TGC TGG GAA TGG TGA AGT G; R1: GGA AGG TAG AGA AGG TGG TAG A; F2: GAA AGC AGG AAA TGA AGA GCA TC; R2: GTT GCA GCG TGG AAA AGG; F3: GCT CAC TCC AGG GCA GCT GCA GCT GCT GCT; R3: TCA CGC ATG CTG GCT CTT AGG GTG TGG CCC) and β-actin (forward: 5′-ACTGTCGAGTCGCGTCCA-3′; reverse: 5′-GTCATCCATGGCGAACTGGT-3′).

Statistics

Between-group comparisons. A repeated measures ANOVA was run at each frequency of stimulation for each AP parameter of interest

(maximum rate-of-rise, peak amplitude, 40% decay, 80% decay, and maximum repolarization). The independent variable was group, which included WT fibers, transgenic R6/2 Huntington's disease (R6/2) fibers, and WT fibers exposed to 9-AC and Ba^{2+} to inhibit ClC-1 and Kir (9-AC/Ba^{2+}). The repeated measure was AP number. The repeated measure accounts for potentially correlated measurements from the same muscle fiber across APs. A random effect for mouse was also included to account for potentially correlated measurements between fibers from the same mouse at each AP. An autoregressive covariance structure, which allows observations further apart in time to be less highly correlated than observations closer together in time, was found to be the best fit by Akaike's Information Criterion (AIC). Denominator degrees of freedom were calculated via the Kenward-Roger degrees of freedom approximation (35). A flow chart of the statistical procedure for assessing between-group effects is shown in Fig. 1.

The presence of a two-way interaction between group and AP number was tested first. A significant interaction indicates that the mean difference between groups was not constant across all APs. When a significant interaction was not present, the interaction term was removed, and the means were directly compared using Tukey's post hoc multiple comparison procedure. In the presence of a significant interaction, a series of repeated-measures ANOVAs were run for each pairwise combination of groups. When there was no significant interaction for a pairwise combination of groups, the groups were compared directly using an ANOVA. When there was a significant interaction between pairs of groups, post hoc multiple comparisons were carried out for each AP number via the Bonferroni sequentially rejective multiple comparison procedure (30). The procedure ensures that the type I error rate for each ANOVA is at most $\alpha = 0.05$.

Within-group comparisons. A repeated measures ANOVA was run for each AP parameter of interest to determine whether the parameter changed over the time course of the AP train. An independent variable for group (WT, R6/2, 9-AC/Ba^{2+}) was not included, since a separate ANOVA was run within each group at each frequency. Therefore, there was only the repeated measure for AP and the random effect for mouse. An autoregressive covariance structure was once again found to be the best fit by AIC. Denominator degrees of freedom were calculated via the Kenward-Roger degrees of freedom approximation (35). All APs in the train were compared with the first single AP recorded before the train, with Bonferroni's sequentially rejective multiple comparison procedure being used to control the type I error rate for the pairwise post hoc comparisons.

RESULTS

Action potentials (APs) were recorded from flexor digitorum brevis and interosseous muscle fibers using two intracellular microelectrodes (a voltage-sensing and a current-passing electrode) from R6/2 mice and their age-matched WT littermates. Because ClC-1 and Kir currents have been shown to be reduced in R6/2 skeletal muscle by ~70% and 30%, respectively (44, 68), APs were measured from WT fibers in the presence of 9-AC (30 μM) and Ba^{2+} (750 nM). The inhibition of ClC-1 and Kir currents by 30 μM 9-AC and 750 nM Ba^{2+} was based on dose-response curves obtained from rodent muscle (47, 51) and used to mimic the conditions observed in R6/2 fibers. AP train comparisons between WT, R6/2, and WT fibers in the presence of 9-AC and Ba^{2+} (9-AC/Ba^{2+}) were analyzed quantitatively by using the statistical method diagramed in Fig. 1. Each AP was analyzed for the maximum rate-of-rise, peak amplitude, 40% decay, 80% decay, and maximum repolarization (Fig. 2*A*, *top* and *middle*). The maximum rate-of-rise was defined by the maximum slope of the AP rising phase, as determined by the first derivative of each AP (Fig. 2*A*, *middle*). The peak amplitude was the peak voltage above 0 mV. The 40% and 80% decay was the duration between the peak amplitude and the voltage at which the falling phase of the AP decayed to 40% or 80% of the total voltage, the total voltage being the difference between the peak amplitude of each AP and the baseline membrane potential (approximately −85 mV). The maximum repolarization is the most negative voltage after each AP. Each AP was evoked by a 0.2-ms current stimulus (Fig. 2*A*, *bottom*).

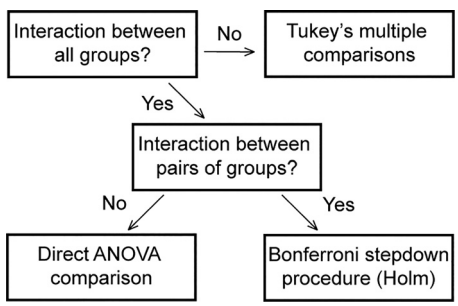

Fig. 1. Statistical methodology for between-group comparison.

Single Action Potential Analysis

To assess single APs, we examined an isolated AP that was recorded before the first 20-Hz AP train from each fiber. This AP was not affected by any physiological changes that may have occurred during AP train recordings. Figure 2*B* shows the average single AP for WT, R6/2, and 9-AC/Ba^{2+} fibers, and Fig. 2, *C–F* shows boxplots of the average maximum rate-of-rise, peak amplitude, 40% decay, and 80% decay. The maximum repolarization was not analyzed because the voltage potential was allowed to return to rest (approximately −85 mV) after each single AP. The results show that the peak amplitude of R6/2 APs was significantly lower (23.68 ± 3.50 mV) than both WT (37.06 ± 2.89 mV) and 9-AC/Ba^{2+} (43.99 ± 3.58 mV) (Fig. 2*C*). This was consistent with the maximum rate-of-rise, which, although not reaching statistical significance, trended lower in R6/2 fibers (244.4 ± 33.23 mV/ms) compared with both WT (320.56 ± 27.40 mV/ms) and 9-AC/Ba^{2+} (309.43 ± 34.82 mV/ms) (Fig. 2*D*). The difference in the R6/2 AP falling phase relative to WT and 9-AC/Ba^{2+} was more apparent. The 40% decay time was significantly higher in R6/2 fibers (2.72 ± 0.17 ms) compared with both WT (1.48 ± 0.14 ms) and 9-AC/Ba^{2+} (1.15 ± 0.16 ms) (Fig. 2*E*). Similarly, the 80% decay time was significantly higher in R6/2 fibers (11.16 ± 0.61 ms) compared with WT (4.72 ± 0.53 ms) and 9-AC/Ba^{2+} (3.50 ± 0.55 ms) (Fig. 2*F*). The decrease in the R6/2 AP peak amplitude suggests a Na^+ channel defect, and the increase in decay time suggests a K^+ channel defect. Because the peak amplitude and decay time of 9-AC/Ba^{2+} APs were not significantly different from WT, reduced ClC-1 and Kir currents do not likely explain the differences between R6/2 and WT APs for these parameters.

Peak Amplitude and Maximum Repolarization

Trains of APs were recorded with increasing stimulation frequency (20 to 40 to 60 Hz). Representative WT and R6/2 60-Hz train recordings are shown in Fig. 3*A*, *left* and *right*, respectively; *insets* show the first AP in the train with the peak

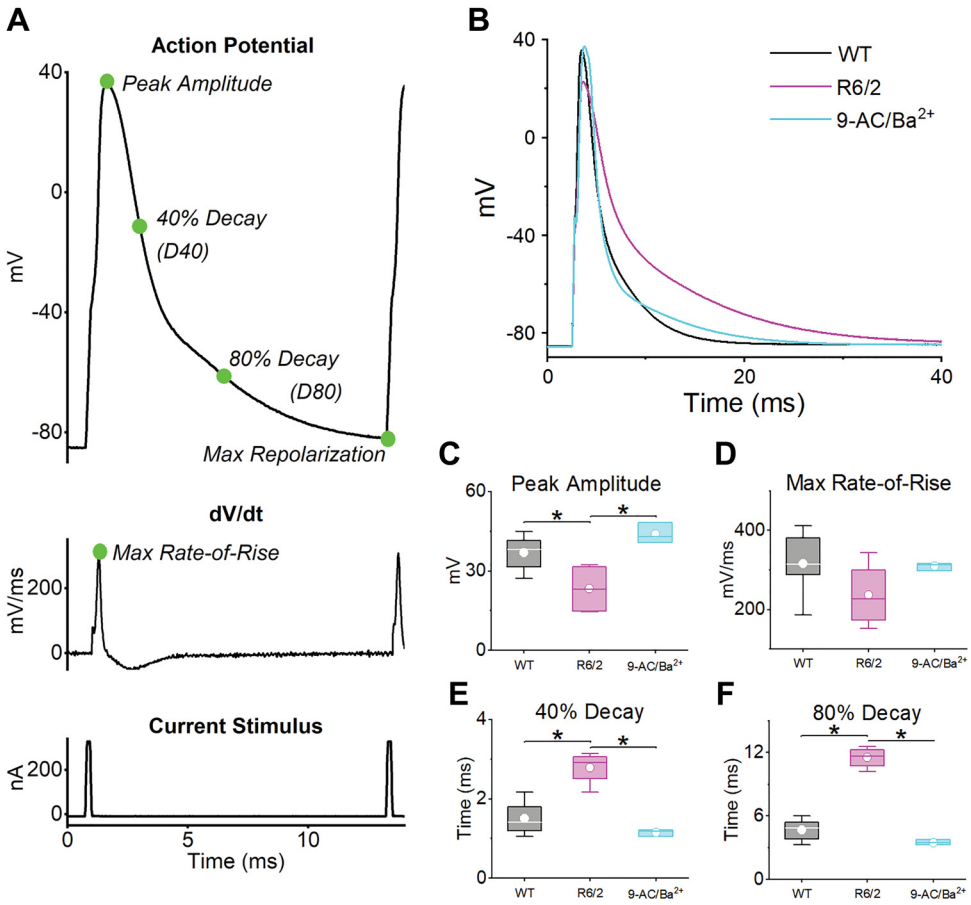

Fig. 2. Action potential (AP) parameters and single AP analysis. *A*: representative AP with peak amplitude, 40% decay, 80% decay, and maximum repolarization labeled (*top*). The maximum rate-of-rise (dV/d*t*) was determined by taking the first derivative of the AP (*middle*). Also shown is the 0.2-ms current pulse used to stimulate each AP (*bottom*). *B*: average single AP for wild-type [WT; $n = 6$ mice (3 male and 3 female), 17 fibers], R6/2 [$n = 4$ mice (2 male and 2 female), 13 fibers], and 9-AC/Ba^{2+} [$n = 3$ mice (3 females), 16 fibers]. *C* –*F*: box plots for (*C*) peak amplitude (WT vs. R6/2 $P = 0.0358$, WT vs. 9-AC/Ba^{2+} $P = 0.34$, and R6/2 vs. 9-AC/Ba^{2+}, $P = 0.0087$); (*D*) maximum rate-of-rise ($P = 0.25$), (*E*) 40% decay (WT vs. R6/2 $P = 0.0008$, WT vs. 9-AC/Ba^{2+}, $P = 0.33$, and R6/2 vs. 9-AC/Ba^{2+}, $P = 0.0007$); and (*F*) 80% decay (WT vs. R6/2 $P < 0.0001$, WT vs. 9-AC/Ba^{2+}, $P = 0.26$, and R6/2 vs. 9-AC/Ba^{2+}, $P < 0.0001$). Data compared using a one-way ANOVA, and box plots show the 25th and 75th percentile (box), mean (dot), median (line), and 1.5 interquartile range (error bars). The horizontal lines with an asterisk indicate a significant difference ($\alpha = 0.5$).

amplitude and max repolarization labeled. Over the duration of the trains, there were significant changes in peak amplitude within the WT, R6/2, and 9-AC/Ba^{2+} groups at 20, 40, and 60 Hz (Table 1). This was determined by comparing each AP in the train to the single AP recorded before each train (Fig. 3*A*). To compare WT, R6/2, and 9-AC/Ba^{2+} AP trains, we first tested for an interaction (Fig. 1). Because there was no significant interaction between the three groups for peak amplitude at 20 Hz ($P = 0.56$ for 20-Hz 3-group interaction; Fig. 3*B*), all three groups were compared using Tukey's multiple comparisons procedure, which treats each train as a whole. As shown in Fig. 3*B*, the peak amplitude of R6/2 APs at 20 Hz was significantly lower than both WT and 9-AC/Ba^{2+}, whereas WT and 9-AC/Ba^{2+} APs were not different from each other. At 40 Hz, the peak amplitude remained significantly lower in R6/2 fibers compared with WT and 9-AC/Ba^{2+}, and there was no significant difference between WT and 9-AC/Ba^{2+} fibers ($P = 0.95$ for 3-group interaction; Fig. 3*B*).

For the peak amplitude at 60 Hz, there was a significant interaction between all three groups ($P < 0.0001$ for 3-group interaction; Fig. 3*B*), which implies that the mean difference between groups was not constant across all APs. Therefore, we determined whether there was an interaction between pairs of groups (Fig. 1). There was no significant interaction between WT and 9-AC/Ba^{2+}, so these groups were compared directly, yielding no significant difference ($P = 0.32$ for pairwise interaction; Fig. 3*B*). A significant pairwise interaction between WT and R6/2 ($P < 0.0001$) and between R6/2 and 9-AC/Ba^{2+} ($P < 0.0001$) led to the more strict Bonferroni multiple comparisons procedure, which also yielded no significant differences (Fig. 2*B*). The primary interaction between all three groups was driven by the sudden drop in peak amplitude from the first AP in the train to the second AP in the train in R6/2 fibers (Fig. 3*B*). This abrupt decrease likely occurred because of the corresponding depolarization in membrane potential (shift in maximum repolarization), which would cause fast inactivation of the skeletal muscle voltage-gated Na^+ channel, $Na_V1.4$ (12, 19). When the data set was analyzed from the second AP onward (AP2-300), the interaction was no longer significant ($P = 0.22$ for 60-Hz 3-group interaction). Tukey's multiple comparison procedure was then employed for AP2-300 and, consistent with the 20 and 40 Hz trains, the peak amplitude of R6/2 APs at 60 Hz was significantly lower than both WT ($P = 0.008$) and 9-AC/Ba^{2+} ($P = 0.029$). In addition, WT was not significantly different from 9-AC/Ba^{2+} ($P = 0.34$). Overall, the peak amplitude of R6/2 APs was consistently reduced compared with WT and 9-AC/Ba^{2+}. Because of the similarity between WT and 9-AC/Ba^{2+}, the decrease in ClC-1 and Kir currents do not likely explain the reduction in R6/2 peak amplitude.

The maximum repolarization was the most negative potential at the end of each AP and describes the extent of repolarization before the next AP in the train (Fig. 3*C*). During each train, there were significant changes in the maximum repolarization within the WT, R6/2, and 9-AC/Ba^{2+} groups at 20, 40,

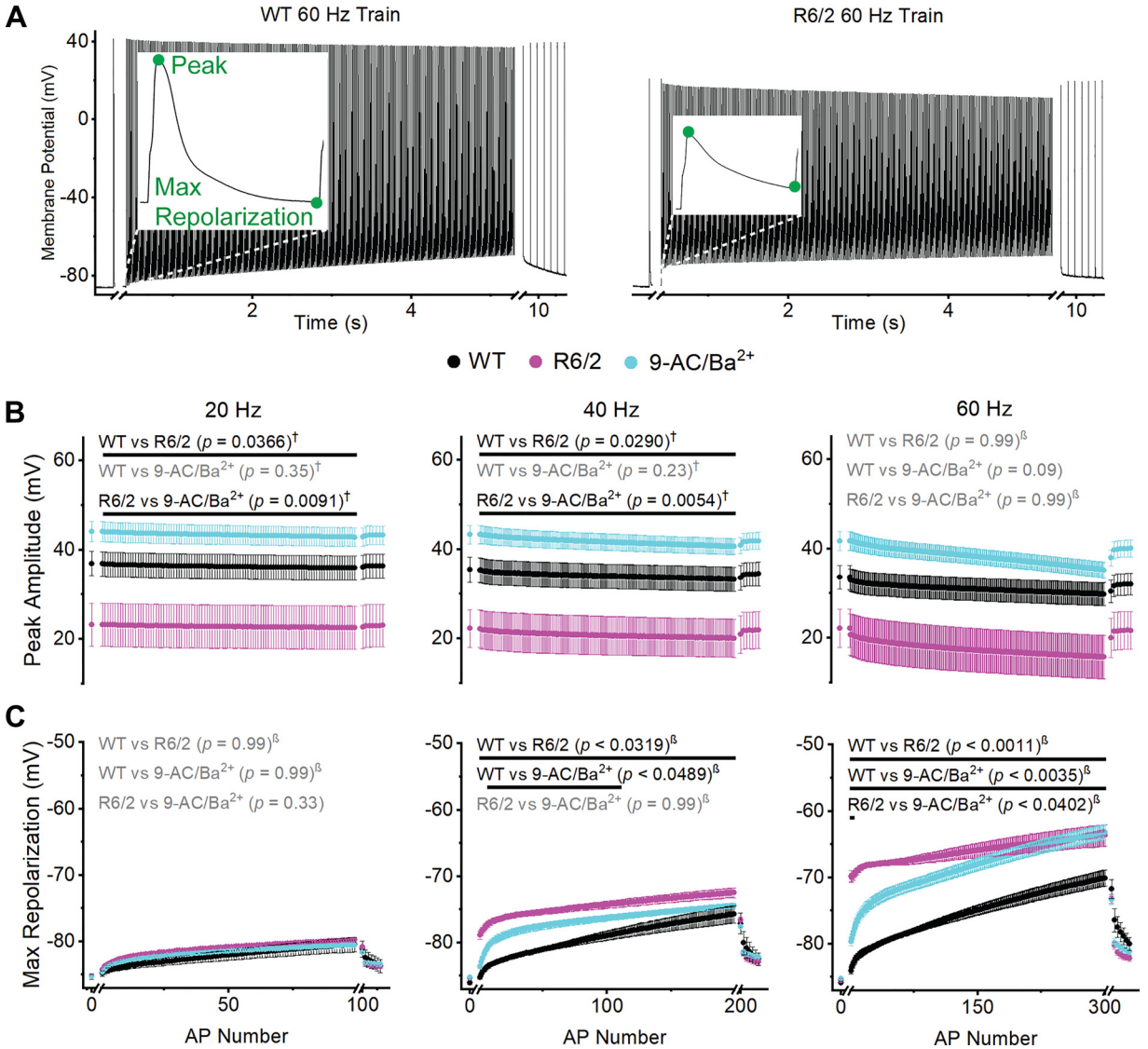

Fig. 3. Action potential (AP) peak amplitude and maximum repolarization. *A*: representative wild-type (WT; *left*) and R6/2 (*right*) 60-Hz AP trains with peak amplitude and maximum repolarization labeled (*insets*). The *x*-axis breaks separate the 1st single AP and recovery APs from the train. *B* and *C*: graph of average peak amplitude (*B*) and maximum repolarization (*C*) at 20-Hz (*left*), 40-Hz (*middle*), and 60-Hz (*right*) for WT [n = 17 fibers (20 and 40 Hz) and 16 fibers (60 Hz) from 6 mice (3 males and 3 females)], R6/2 [n = 13 fibers (20 Hz), 11 fibers (40 Hz), and 12 fibers (60 Hz) from 4 mice (2 males and 2 females)], and 9-AC/Ba^{2+} [n = 16 fibers (20 Hz and 40 Hz) and 15 fibers (60 Hz) from 3 female mice]. Each AP is shown as an average ± SE. Black font signifies a significant difference and gray font indicates no significant difference between groups. Black lines indicate which APs were significantly different. † = Tukey's comparison procedure. β=stepdown Bonferroni comparison procedure. No symbol = direct comparison.

and 60 Hz (Table 1). Between groups, there was no significant difference in the maximum repolarization at 20 Hz (P < 0.0001 for 3-group interaction; Fig. 3*C*). At 40 Hz, the maximum repolarization of R6/2 APs jumped from −85.29 ± 0.16 mV (initial single AP) to −78.83 ± 0.65 mV (AP1 of the train) and continued to depolarize to −72.50 ± 0.74 mV by the end of the train. In contrast, the WT maximum repolarization gradually depolarized from −86.02 ± 0.27 mV to −75.71 ± 1.30 mV over the duration of the train. Thus, the maximum repolarization was significantly more depolarized in R6/2 fibers compared with WT at 40 Hz (P < 0.0001 for 3-group interaction; Fig. 3*C*). In the presence of 9-AC/Ba^{2+}, the maximum repolarization was significantly more depolarized than WT from AP8 to AP110 but not significantly different from R6/2 fibers at any AP in the 40-Hz train (Fig. 3*C*). Overall, the R6/2 maximum repolarization was more similar to 9-AC/Ba^{2+} than WT at 40 Hz.

A striking feature of the maximum repolarization at 60 Hz was the large step from −85.50 ± 0.26 mV after the single AP to −69.79 ± 0.86 mV for AP1 in R6/2 fibers (Fig. 3*C*). A similar but less dramatic step was observed in the presence of 9-AC/Ba^{2+}. By the end of the 60-Hz train, the maximum repolarizations of R6/2 and 9-AC/Ba^{2+} fibers were −63.64 ± 1.65 and −63.15 ± 1.07 mV, respectively. In contrast, the maximum repolarization of WT fibers at 60 Hz underwent a more gradual change from −85.53 ± 0.25 mV at baseline to −70.05 ± 1.21 mV by the end of the train, making it significantly different from R6/2 and 9-AC/Ba^{2+} fibers throughout the 60 Hz train (P < 0.0001 for 3-group interaction; Fig. 3*C*). Highlighting their similarities, the R6/2 and 9-AC/Ba^{2+} fibers

Table 1. *Within-group AP comparison*

Group (Frequency)	Peak Amplitude	Maximum Repolarization	Maximum Rate of Rise	40% Decay	80% Decay
WT					
20 Hz	AP 2 onward ($P < 0.0099$)	All APs ($P < 0.0001$)	AP 3–27 ($P < 0.0413$)	None	AP 2–8 ($P < 0.0094$)
40 Hz	All APs ($P < 0.0035$)	AP 2 onward ($P < 0.0443$)	All APs ($P < 0.0091$)	None	AP 54 onward ($P < 0.0487$)
60 Hz	AP 2 onward ($P < 0.0009$)	All APs ($P < 0.0001$)	All APs ($P < 0.0001$)	None	AP 66 onward ($P < 0.0494$)
R6/2					
20 Hz	None	All APs ($P < 0.0001$)	All APs ($P < 0.0050$)	None	All APs ($P < 0.0001$)
40 Hz	AP 2 onward ($P < 0.0018$)	All APs ($P < 0.0027$)	All APs ($P < 0.0023$)	AP 44 onward ($P < 0.0496$)	All APs ($P < 0.0001$)
60 Hz	AP 2 onward ($P < 0.0001$)	All APs ($P < 0.0001$)	AP 2 onward ($P < 0.0001$)	All APs ($P < 0.0057$)	All APs ($P < 0.0001$)
9-AC/Ba^{2+}					
20 Hz	AP 41 onward ($P < 0.0497$)	All APs ($P < 0.0001$)	All APs ($P < 0.0003$)	None	All APs ($P < 0.0001$)
40 Hz	AP 13 onward ($P < 0.0421$)	All APs ($P < 0.0001$)	All APs ($P < 0.0001$)	All APs ($P < 0.0060$)	All APs ($P < 0.0001$)
60 Hz	AP 6 onward ($P < 0.0147$)	All APs ($P < 0.0001$)	All APs ($P < 0.0001$)	All APs ($P < 0.0015$)	All APs ($P < 0.0001$)

AP, action potential; WT, wild type. All APs in the train were compared with the first single AP recorded before the train with Bonferroni's sequentially rejective multiple comparison procedure.

were only statistically different at AP1 and AP2 (Fig. 3*C*). Overall, exposure of WT fibers to 9-AC/Ba^{2+} largely replicated the AP maximum repolarization in R6/2 fibers, suggesting that reduced ClC-1 and Kir currents alone can largely explain the shift in the max repolarization of R6/2 APs.

Maximum Rate-of-Rise

The maximum rate-of-rise was the maximum slope of the AP rising phase, which was calculated by taking the first derivative of each AP. Figure 4*A* shows the derivative of the first and last three APs of representative WT (Fig. 4*A*, *left*) and R6/2 (Fig. 4*A*, *right*) 60-Hz trains. Within the 20-, 40-, and 60-Hz AP trains, the maximum rate-of-rise decreased significantly for WT, R6/2, and 9-AC/Ba^{2+} (Table 1). The least dramatic changes occurred in WT fibers at 20 Hz, in which the maximum rate-of-rise significantly decreased only in some APs (Table 1). In comparing groups, it appeared that the R6/2 maximum rate-of-rise was lower than WT and 9-AC/Ba^{2+}

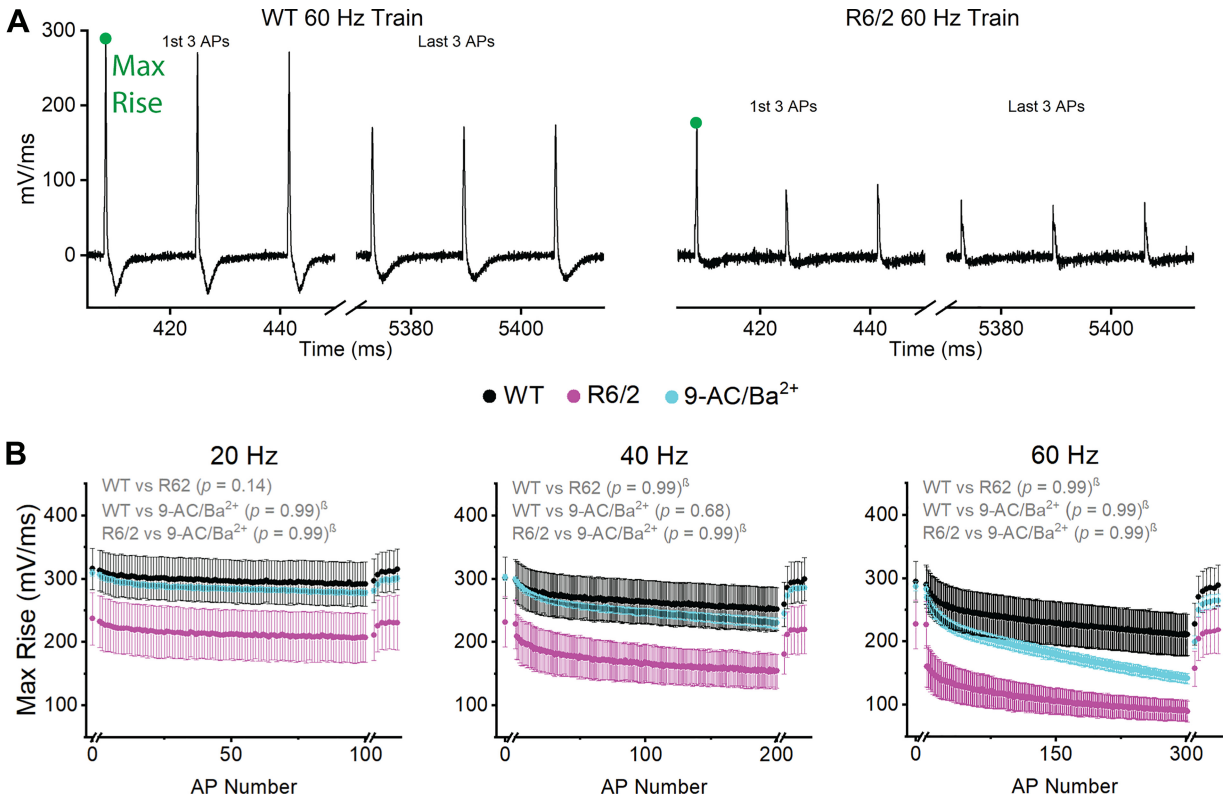

Fig. 4. Action potential (AP) maximum rate-of-rise. *A*: first and last 3 APs from representative wild-type (WT; *left*) and R6/2 (*right*) 60-Hz AP trains with maximum rate-of-rise labeled. The *x*-axis breaks separate the 1st single AP and recovery APs from the train. *B*: graph of maximum rate-of-rise at 20 Hz (*left*), 40 Hz (*middle*), and 60 Hz (*right*) for WT [$n = 17$ fibers (20 Hz and 40 Hz) and 16 fibers (60 Hz) from 6 mice (3 males and 3 females)], R6/2 [$n = 13$ fibers (20 Hz), 11 fibers (40 Hz), and 12 fibers (60 Hz) from 4 mice (2 males and 2 females)], and 9-AC/Ba^{2+} [$n = 16$ fibers (20 Hz and 40 Hz) and 15 fibers (60 Hz) from 3 female mice]. Data are shown as average ± SE. Black font signifies a significant difference between groups. Gray font signifies no significant difference. Black lines signify which APs are significantly different between groups. †=Tukey's comparison procedure. β=stepdown Bonferroni comparison procedure. No symbol = direct comparison.

(Fig. 4). In response to repetitive stimulation, the R6/2 maximum rate-of-rise decreased by 11% at 20 Hz, 33% at 40 Hz, and 60% at 60 Hz. The change in R6/2 maximum rate-of-rise was approximately twofold more than WT, which decreased by 7% at 20 Hz, 15% at 40 Hz, and 27% at 60 Hz. The 9-AC/Ba^{2+} maximum rate-of-rise began at levels close to WT and decreased by 9% at 20 Hz, 23% at 40 Hz, and 50% at 60 Hz. However, the maximum rate-of-rise was not significantly lower in R6/2 fibers compared with WT or 9-AC/Ba^{2+} at any frequency, based on the direct ANOVA comparison and the stepdown Bonferroni procedure (Fig. 4*B*). To assess whether this was due to high variability or the strict correction made to the *P* values by the multiple comparison procedure in the presence of between groups interactions, we compared specific APs using a standard one-way ANOVA. The maximum rate-of-rise for AP1 was not significantly different between WT, R6/2, and 9-AC/Ba^{2+} fibers at 20 Hz ($P = 0.24$), 40 Hz ($P = 0.30$), or 60 Hz ($P = 0.36$). Similarly, the maximum rate-of-rise of the last AP in the train was not significantly different between R6/2, WT, and 9-AC/Ba^{2+} at 20 Hz (AP100, $P = 0.23$) or 40 Hz (AP200, $P = 0.11$). At 60 Hz, there was a substantial drop in maximum rate-of-rise at AP2 in R6/2 fibers, which prompted us to test for differences at AP2 and AP300 (Fig. 4*B*). Indeed, the R6/2 maximum rate-of-rise was significantly lower than WT at AP2 (R6/2: 160.88 ± 32.66 mV/ms; WT: 285.47 ± 32.65 mV/ms; $P = 0.0406$) and at AP300 (R6/2: 89.64 ± 16.90 mV/ms; WT: 210.64 ± 33.13 mV/ms; $P = 0.02807$). The WT maximum rate-of-rise was not significantly different from 9-AC/Ba^{2+} at AP2 (269.44 ± 9.03 mV/ms, $P = 0.14$) or AP300 (141.54 ± 7.84 mV/ms, $P = 0.52$). Thus, whereas high variability drove the lack of statistical significance in AP maximum rate-of-rise between groups at 20 and 40 Hz, there was evidence that the AP maximum rate-of-rise was lower in R6/2 fibers compared with WT at 60 Hz. Exposure of WT fibers to 9-AC/Ba^{2+} had little effect on the AP maximum rate-of-rise, suggesting that reduced ClC-1 and Kir currents in R6/2 skeletal muscle do not explain changes in the AP rising phase during repetitive firing.

Falling Phase

The falling phase of each AP consisted of a fast and slow portion. The fast portion was analyzed using the 40% decay time and the slow portion analyzed using the 80% decay time, both from the peak. APs from the beginning and end of a representative WT and R6/2 60 Hz train are shown in Fig. 5*A*, *left* and *right*, respectively, with the 40% (D40) and 80% (D80) decay points labeled. Within all groups, the 40% decay did not significantly change during 20-Hz trains and remained constant in WT fibers at all frequencies (Table 1). Within the R6/2 and 9-AC/Ba^{2+} groups, the 40% decay was significantly prolonged over the duration of the 40-Hz and 60-Hz trains (Table 1). Between groups, the 40% decay of R6/2 APs was significantly prolonged compared with WT and 9-AC/Ba^{2+} at 20-, 40-, and 60-Hz stimulation, whereas the 40% decay in WT fibers was not significantly different from 9-AC/Ba^{2+} fibers ($P = 0.84$ for 3-group interaction; Fig. 5*B*).

The 80% decay time significantly increased within all groups at all frequencies (Table 1). The between-group comparison for the 80% decay was similar to that of the 40% decay. R6/2 APs had a significantly higher decay time than both WT and 9-AC/Ba^{2+} at all frequencies (Fig. 5*C*). Because of the shift in the maximum repolarization (Fig. 3*C*), many of the APs from R6/2 and 9-AC/Ba^{2+} fibers at 60 Hz did not decay to 80% before the next AP fired, especially by the end of the train. Therefore, seven of the R6/2 and 10 of the 9-AC/Ba^{2+} fibers could not be used for the 80% decay results. Overall, these data show that there was an increase in both the 40% and 80% AP decay time in R6/2 muscle fibers compared with WT, which was not explained by the partial block of ClC-1 and Kir currents, suggesting a K^+ current defect.

Increasing R6/2 Peak Amplitude to WT Levels

Previous studies suggest that a decrease in AP peak amplitude can increase the duration of the falling phase (6, 29). To test this, we experimentally increased the peak amplitude of R6/2 APs (high-stim) to ~50 mV, which was slightly above WT levels, by increasing the amplitude of the stimulus pulse in 25-nA intervals (Fig. 6*A*). Because the high-stim APs had different peak characteristics from normal APs (Fig. 6*A*), the 40% and 80% decay for the high-stim APs were not comparable with those of normal APs. Thus, to examine the falling phase, we determined the maximum rate-of-decay using the first derivative of each high-stim AP (Fig. 6, *A* and *B*). We focused on the decay rates that occurred after the rapid voltage changes caused by the high-stimulus current had subsided, shown in Fig. 6, *A* and *B* as the region bracketed by dashed vertical lines. This region of the high-stim APs was most comparable with regular APs from WT and R6/2 fibers. As can be seen in Fig. 6*B*, increasing the AP peak had little effect on the rate of repolarization. To better examine the relationship between peak amplitude and falling phase, we plotted the maximum rate-of-decay as a function of peak amplitude for regular WT and R6/2 APs as well as high-stim R6/2 APs; each group was fit with a line (Fig. 6*C*). The WT slope (1.72 ± 0.16 ms^{-1}) was greater than the R6/2 slope (0.79 ± 0.07 ms^{-1}), suggesting that the WT maximum rate-of-decay was more steeply dependent on peak amplitude than the R6/2 maximum rate-of-decay. In addition, the high-stim R6/2 slope (0.50 ± 0.14 ms^{-1}) was lower than the R6/2 slope, suggesting that the prolonged falling phase of R6/2 APs was not caused by a decrease in peak amplitude. Most likely, the prolonged repolarization of R6/2 muscle was caused by a reduction in voltage-dependent K^+ current.

Decreased Voltage-Gated K^+ Channel mRNA in HD Skeletal Muscle

To determine whether the prolonged falling phase of R6/2 APs was due to reduced voltage-gated K^+ channel (K_V) current, we measured the mRNA expression levels of three K_V genes reported to be expressed in mouse skeletal muscle (16, 39, 66). We found that, compared with WT, $K_V1.5$ was reduced by 43% and $K_V3.4$ was reduced by 81% in R6/2 interosseous skeletal muscle (Fig. 7). We also tested three different primers sets for $K_V1.4$. The very high C_T levels suggested that $K_V1.4$ was expressed at very low levels in both WT and R6/2 skeletal muscle (not shown). Overall, the reduction in $K_V1.5$ and $K_V3.4$ mRNA helps explain the prolonged decay time of R6/2 APs.

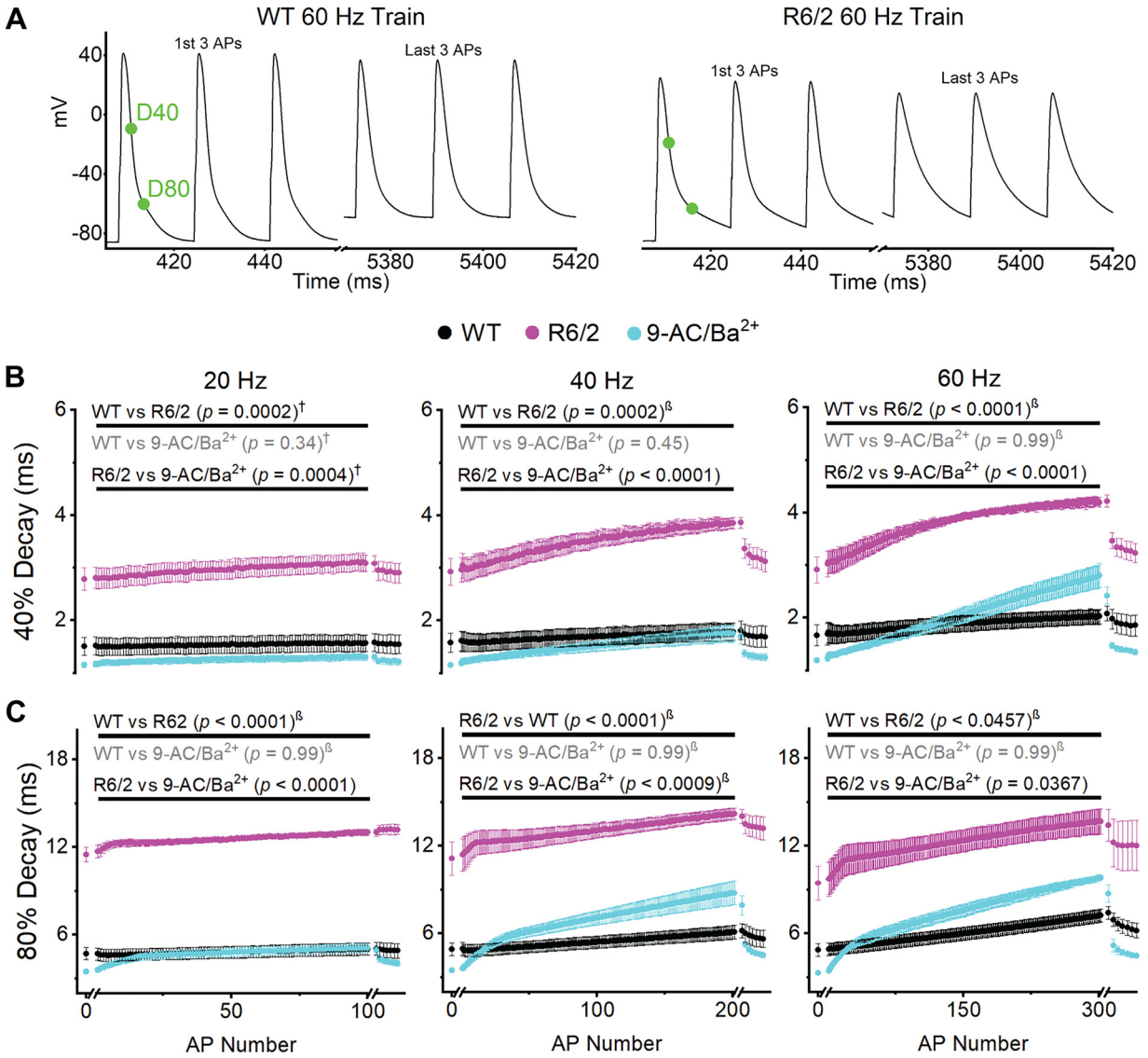

Fig. 5. 40% Decay (D40) and 80% decay (D80). *A*: first and last 3 action potentials (APs) from representative wild-type (WT; *left*) and R6/2 (*right*) 60-Hz AP trains with points of analysis labeled. The *x*-axis breaks separate the 1st single AP and recovery APs from the train. *B*: graph of 40% decay for WT [n = 17 fibers (20 Hz and 40 Hz) and 16 fibers (60 Hz) from 6 mice (3 males and 3 females)], R6/2 [n = 13 fibers (20 Hz), 11 fibers (40 Hz), and 12 fibers (60 Hz) from 4 mice (2 males and 2 females)], and 9-AC/Ba^{2+} [n = 16 fibers (20 Hz and 40 Hz) and 14 fibers (60 Hz) from 3 female mice. *C*: graph of 80% decay for WT [n = 17 fibers (20 Hz and 40 Hz) and 15 fibers (60 Hz) from 6 mice], R6/2 [n = 13 fibers (20 Hz), 9 fibers (40 Hz), and 5 fibers (60 Hz) from 4 mice], and 9-AC/Ba^{2+} [n = 16 fibers (20 Hz and 40 Hz) and 4 fibers (60 Hz) from 3 mice]. For *B* and *C*, decay values shown for 20-Hz (*left*), 40-Hz (*middle*), and 60-Hz (*right*) stimulation. Data shown as average ± SE. Black font signifies a significant difference between groups. Gray font signifies no significant difference. Black lines signify which APs are significantly different between groups. †=Tukey's comparison procedure. β=stepdown Bonferroni comparison procedure. No symbol = direct comparison.

Action Potential Recovery

Following each AP train, 7 APs were recorded at 0.5 Hz to assess recovery from the train. The first recovery AP was recorded 125 ms after the last AP in the train. Thus, recovery occurred over two phases, a fast phase within the first 125 ms after the train and a more gradual phase during the 0.5-Hz recovery period, which followed an exponential time course (Fig. 8). Full recovery of each AP parameter did not often occur within the ~15-s recovery period. However, as can be seen by comparing the first data points of each frequency panel in Figs. 2–5, full recovery was achieved during the 1- to 3-min rest period between the 20-, 40-, and 60-Hz trains.

For analysis of the peak amplitude and maximum rate-of-rise recovery, the last AP in the train was set to zero, and the recovery values were normalized to the first single AP. The recovery values were fitted with the equation

$$y = y_0 + A^* \left(1 - e^{-\frac{x}{\tau}}\right)$$

where y_0 = y-intercept, A = amplitude, and τ = time constant. For the analysis of the maximum repolarization, 40% decay, and 80% decay recovery, the first single AP was set to zero, and recovery values were normalized to the last AP in the train. The recovery values were fitted with the equation

$$y = y_0 + A^* \left(e^{-\frac{x}{\tau}}\right)$$

where y_0 = y-intercept, A = amplitude, and τ = time constant. The τ and R^2 values for all fitted curves are shown in Table 2.

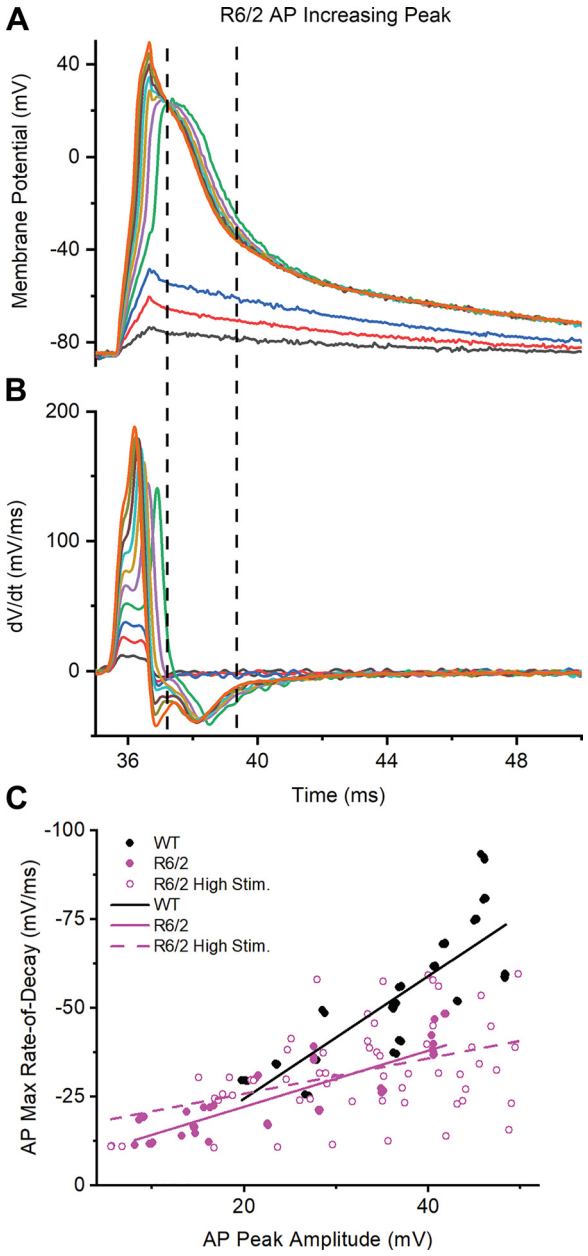

Fig. 6. Relationship between action potential (AP) peak amplitude and maximum rate-of-decay. *A*: representative recording of R6/2 APs with increasing peak amplitudes. *B*: first derivative of the APs from *A* to determine maximum rate-of-decay. Traces in *A* and *B* are color-coded and the dotted lines bracket the region used for analysis. *C*: plot of AP maximum rate-of-decay vs. AP peak amplitude for wild-type [WT; $n = 6$ mice (3 males and 3 females), 17 fibers, 57 APs], R6/2 [$n = 4$ mice (2 males and 2 females), 13 fibers, 46 APs], and R6/2 high stimulation (high stim; $n = 2$ male mice, 11 fibers, 59 APs) with linear regression lines.

Note that recovery was not analyzed for AP parameters that did not significantly change during a train in the within groups comparison (Table 1), such as the peak amplitude of APs in R6/2 fibers during 20-Hz stimulation.

As shown in Fig. 8*A*, the peak amplitude in R6/2 fibers recovered to a greater extent than in WT and 9-AC/Ba^{2+} fibers at 40 and 60 Hz. The rapid jump in peak amplitude from the last AP in the train (open blue circle) to the first recovery AP (initial 125-ms recovery period) was more pronounced in R6/2 fibers compared with WT and 9-AC/Ba^{2+} and was larger with increasing frequency. In addition to the initial jump in recovery, the time constant values (Table 2) describe a faster recovery in R6/2 fibers compared with WT and 9-AC/Ba^{2+}. The rapid 125-ms recovery of the peak amplitude in R6/2 fibers could be partially explained by relief of $Na_V1.4$ fast inactivation, as would result from a quick recovery of the maximum repolarization.

The recovery of maximum repolarization (Fig. 8*B*) was most similar between R6/2 and 9-AC/Ba^{2+} fibers, both of which differed from WT fibers, especially at 60 Hz. At 40 Hz and 60 Hz, the R6/2 and 9-AC/Ba^{2+} maximum repolarization recovered more than WT during the initial 125 ms and had a faster time constant (Table 2). Also, at 60 Hz, the R6/2 and 9-AC/Ba^{2+} fibers had a more complete overall recovery during the 15-s recovery phase compared with WT. The 9-AC/Ba^{2+} recovery became closer to R6/2 with increasing frequency, where, at 60 Hz, they became nearly identical (Fig. 8*B*).

The recovery of the maximum rate-of-rise was similar between groups at all frequencies in terms of time constant (Table 2) and extent of recovery but differed in rapid initial recovery (Fig. 8*C*). The fast recovery at 60 Hz in R6/2 and 9-AC/Ba^{2+} fibers was nearly double that of WT fibers. This is somewhat similar to the trend observed in the peak amplitude recovery and is likely heavily influenced by the maximum repolarization.

Recovery of the 40% decay was analyzed only for the R6/2 and 9-AC/Ba^{2+} fibers at 40 and 60 Hz. This is because there was no statistical change in the 40% decay in WT fibers at any frequency or in R6/2 and 9-AC/Ba^{2+} fibers at 20 Hz (Table 1). Despite significant and apparent differences in the 40% decay between R6/2 and 9-AC/Ba^{2+} fibers at 40 and 60 Hz, there were no clear differences in the initial rapid recovery (Fig. 8*D*) or in the rate of exponential recovery (Table 2).

Recovery of the 80% decay (Fig. 8*E*) differed from the trend observed in the 40% decay. During the first 125 ms after the trains, there was little to no recovery in the 80% decay of R6/2 or 9-AC/Ba^{2+} fibers at any frequency; WT fibers continued to prolong (worsen) during the initial 125-ms recovery period at all frequencies, as indicated by values >1 in Fig. 8*E*. Unexpectedly, after 20-Hz trains, the 80% decay in R6/2 fibers continued to prolong instead of shorten during the 0.5-Hz recovery. This was primarily due to two R6/2 fibers in which

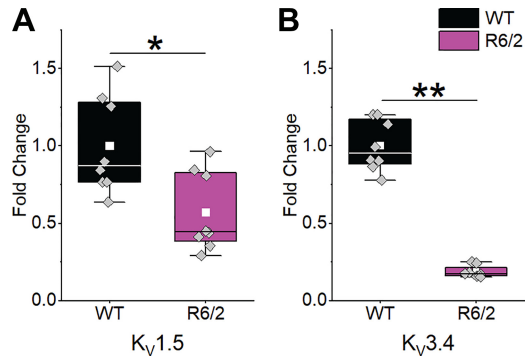

Fig. 7. K_V mRNA expression. The expression of $K_V1.5$ (*A*) and $K_V3.4$ (*B*) relative to β-actin was significantly reduced in R6/2 interosseous muscle [$n = 4$ mice (2 males and 2 females)] compared with wild type [WT; $n = 4$ (2 males and 2 females)]. Data compared using a two-sample *t* test. Columns shown as means ± SE. $^*P = 0.010$; $^{**}P = 1.592 \times 10^{-09}$.

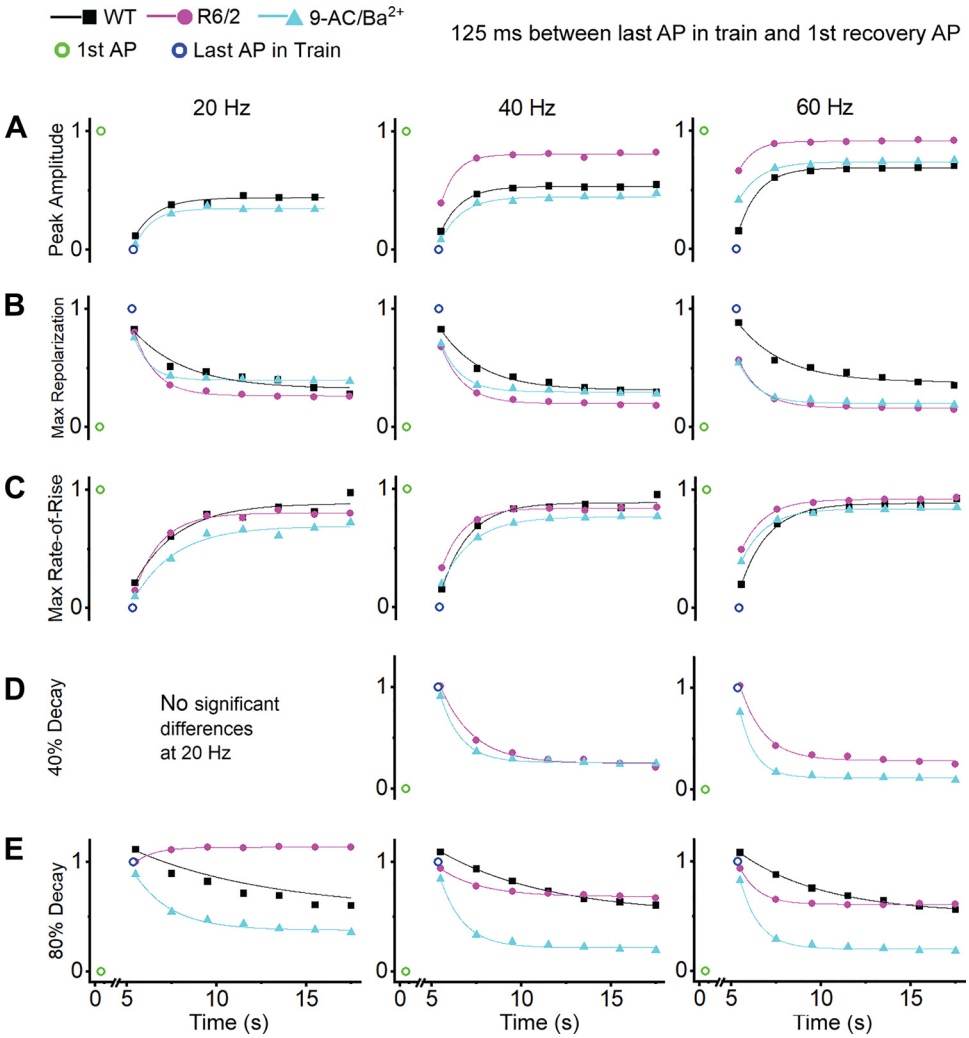

Fig. 8. Recovery action potentials (APs). First single AP (open green circle), last AP in train (open blue circle), and recovery APs for peak amplitude (*A*), maximum repolarization (*B*), maximum rate-of-rise (*C*), 40% decay (*D*), and 80% decay (*E*) at 20 Hz (*left*), 40 Hz (*middle*), and 60 Hz (*right*) with recovery APs fitted with an exponential equation. Recovery was not analyzed for AP parameters that did not significantly change during a train in the within-group comparison. WT, wild type.

the 80% decay did recover. Notably, the peak amplitude, maximum rate-of-rise, 40% decay, and maximum repolarization did recover in these two fibers, suggesting that the 80% decay of APs is controlled separately from the other parameters. Otherwise, the 80% decay of WT APs recovered at the slowest rate during the 0.5-Hz recovery (Table 2). In R6/2 and 9-AC/Ba^{2+} fibers, the AP 80% decay recovered at a similar rate during the 0.5-Hz train, although the extent of recovery

Table 2. *Curve fit values for AP recovery*

	WT		R6/2		9-AC/Ba^{2+}	
	$\tau \pm$ SE, s	R^2	$\tau \pm$ SE, s	R^2	$\tau \pm$ SE, s	R^2
20-Hz peak amplitude	1.26 ± 0.27	0.979	N/A	N/A	0.94 ± 0.20	0.988
40-Hz peak amplitude	1.15 ± 0.11	0.997	0.83 ± 0.18	0.991	1.20 ± 0.24	0.983
60-Hz peak amplitude	1.13 ± 0.09	0.997	0.84 ± 0.13	0.995	1.21 ± 0.13	0.995
20-Hz maximum repolarization	N/A	N/A	1.19 ± 0.09	0.997	0.85 ± 0.11	0.997
40-Hz maximum repolarization	2.29 ± 0.33	0.987	1.23 ± 0.12	0.996	1.10 ± 0.16	0.993
60-Hz maximum repolarization	2.57 ± 0.52	0.976	1.25 ± 0.11	0.996	1.06 ± 0.17	0.991
20-Hz maximum rate-of-rise	2.42 ± 0.71	0.950	1.46 ± 0.16	0.993	2.31 ± 0.50	0.972
40-Hz maximum rate-of-rise	1.55 ± 0.27	0.984	1.17 ± 0.09	0.997	1.70 ± 0.02	0.999
60-Hz maximum rate-of-rise	1.56 ± 0.19	0.992	1.32 ± 0.11	0.997	1.34 ± 0.10	0.997
20-Hz 40% decay	NA	NA	NA	NA	NA	NA
40-Hz 40% decay	NA	NA	1.80 ± 0.20	0.992	1.14 ± 0.10	0.997
60-Hz 40% decay	NA	NA	1.32 ± 0.16	0.993	0.84 ± 0.09	0.997
20-Hz 80% decay	7.75 ± 2.46	0.983	1.08 ± 0.12	0.995	2.05 ± 0.31	0.986
40-Hz 80% decay	6.08 ± 0.41	0.999	2.27 ± 0.36	0.984	1.28 ± 0.14	0.994
60-Hz 80% decay	4.75 ± 0.38	0.997	1.03 ± 0.05	0.999	1.06 ± 0.12	0.995

The $\tau \pm$ SE and R^2 values for curves fitted to recovery action potentials (APs). NA, recovery not analyzed because the respective AP parameters did not significantly change during a train in the within-group comparison; WT, wild type.

was less in R6/2 fibers. Overall, the 80% decay recovery was greater in the 9-AC/Ba^{2+} fibers than in WT and R6/2.

DISCUSSION

Our previous work revealed that skeletal muscle from transgenic R6/2 Huntington's disease mice is hyperexcitable owing to decreased ClC-1 and Kir currents (44, 68). In this study, we examined action potential (AP) repetitive firing in R6/2 skeletal muscle, and by pharmacologically blocking ClC-1 and Kir currents in WT muscle to R6/2 levels, we show which changes in R6/2 APs were caused by decreased ClC-1 and Kir currents. This led us to discover a decrease in voltage-gated K^+ channel (K_V) mRNA expression in R6/2 skeletal muscle. Our analyses also provide insights into the dynamic changes that occur during repetitive firing in WT muscle.

Action Potentials in Huntington's Disease Skeletal Muscle

In isolation and during repetitive firing, R6/2 skeletal muscle APs had significantly lower peaks and significantly prolonged decay times and tended to have a slower rates-of-rise compared with WT APs. The partial block of ClC-1 and Kir currents in WT muscle (9-AC/Ba^{2+}) did not replicate these changes, which is consistent with the established roles of Cl^- and K^+ currents in maintaining the resting membrane potential of skeletal muscle fibers (27). Indeed, the extent to which the membrane potential returned to rest after each AP during repetitive firing (maximum repolarization) was significantly attenuated in both R6/2 and 9-AC/Ba^{2+} fibers compared with WT, indicating that reduced ClC-1 and Kir currents in R6/2 muscle cause a shift in maximum repolarization to more depolarized levels. Furthermore, this indicates that the maximum repolarization during AP trains is regulated by ion channels (and perhaps transporters) that are independent from the ion channels that determine the rate of AP repolarization (measured by the 40% and 80% decay in this study).

The most widely accepted explanation for the depolarized shift in maximum repolarization during repetitive stimulation is K^+ accumulation in the transverse tubules (t-tubules), which shifts the Nernst potential for K^+ to cause depolarization of the resting membrane potential (1, 2, 21, 67). Normally, ClC-1-mediated Cl^- current, which accounts for 70–80% of resting muscle membrane conductance, offsets the depolarizing influence of K^+ accumulation and thus lessens the steady depolarization (1, 4, 46, 56, 57). However, when ClC-1 currents are decreased (as in R6/2 muscle) or partially blocked (as in 9-AC/Ba^{2+} muscle), the effect of K^+ buildup is exaggerated. Whether K^+ buildup is the sole cause of the steady depolarization remains unknown.

K^+ buildup in the t-tubules is expected to occur gradually during repetitive firing such that there would be a gradual shift in maximum repolarization if it is the primary driver of the depolarization. Though a gradual shift in maximum repolarization was observed in WT fibers, the depolarized shift was abrupt in R6/2 and 9-AC/Ba^{2+} fibers, particularly at high frequencies of stimulation. We propose that the activation of a subthreshold current may be responsible for this rapid depolarization. For example, persistent inward Na^+ current is a voltage-activated current that is an important trigger of myotonic APs in muscle lacking ClC-1 channels (25, 40). Activation of persistent inward Na^+ current is likely to be increased in R6/2 and 9-AC/Ba^{2+} fibers by the lack of full repolarization following APs. Furthermore, the depolarization caused by persistent inward Na^+ current will be amplified in R6/2 and 9-AC/Ba^{2+} fibers compared with WT fibers because of the increased membrane resistance (44, 68). The combination of increased activation of a subthreshold current and its amplified effect on membrane potential may lead to the sudden lack of repolarization following APs.

The low peak amplitude and tendency toward a slower rate-of-rise observed in R6/2 APs was not likely due to reduced ClC-1 and Kir currents because of the normal rising phase in 9-AC/Ba^{2+} fibers, suggesting the presence of other ion channel defects. The rising phase of an AP, which includes the rate-of-rise and peak amplitude, has classically been attributed to Na^+ influx (28), which in skeletal muscle is mediated by the voltage-gated Na^+ channel $Na_V1.4$ (23). Therefore, it is likely that there is a disruption in $Na_V1.4$ activity in R6/2 skeletal muscle. The disruption is not likely caused by a reduction in the Na^+ equilibrium potential because we controlled the intracellular and extracellular Na^+ concentrations. More likely, there is a decrease in $Na_V1.4$ current or a shift in the voltage dependence of $Na_V1.4$ activation and/or inactivation. There is evidence of altered $Na_V1.4$ activity in other HD cell types. In striatal neurons, the β4-subunit, which is involved in the voltage dependence of Na^+ channel activation, was shown to be downregulated in HD mouse models and human patients (45). Further studies will be needed to determine whether $Na_V1.4$ influences R6/2 APs in skeletal muscle.

The most dramatic difference between R6/2 and WT APs was the decay time. Compared with WT, the falling phase of R6/2 APs was markedly prolonged and was not due to reduced ClC-1 and Kir currents. Prolonged decay has been associated with low peak amplitude (6, 29). However, the low peak of R6/2 APs did not likely cause the prolonged decay time because injecting current to increase the peak of R6/2 APs did not increase the rate-of-decay time. Therefore, since K_V currents are responsible for the falling phase of APs (6, 16), we measured the expression level of $K_V1.5$ and $K_V3.4$ in R6/2 skeletal muscle.

Voltage-Gated K^+ Channel Expression in HD Skeletal Muscle

We found that mRNA levels of $K_V1.5$ and $K_V3.4$ were lower in R6/2 skeletal muscle compared with WT, which helps explain the prolonged decay time we observed in R6/2 APs. Similarly, APs in R6/2 medium spiny neurons have a prolonged decay time and decreased $K_V2.1$ expression (5, 37). There are several factors that may lead to decreased $K_V3.4$ expression in R6/2 skeletal muscle. Skeletal muscle $K_V3.4$ expression decreases in denervated muscle, is higher in fast-twitch muscle fibers, and increases with age until adulthood in mice (66). We can exclude a relation to denervation since morphological, physiological, and molecular experiments have shown that R6/2 skeletal muscle is not denervated (36). Fiber type switching may help explain the reduced $K_V3.4$ levels since a shift to slow and neonatal myosin heavy chain occurs in R6/2 muscle (42, 44, 52, 58). Additionally, we have shown that R6/2 skeletal muscle is not fully matured (44). Thus, it may be that a transition to slow fiber types and disruption in muscle maturation explain the reduced $K_V3.4$ levels. Addition-

ally, transcription factor activity for $K_V3.4$ may be altered in R6/2 skeletal muscle. *Kcna4*, the gene that codes for $K_V3.4$, contains binding sites for Sp-1 and RORα1 (18, 65), transcription factors that have been shown to bind or are thought to bind mutant huntingtin protein (7, 34). This pathway has been linked to the downregulation of proteins such as Kir4.1 and to HD pathology such as dysregulated intracellular Ca^{2+} signaling (7, 34).

$K_V1.5$ expression changes throughout skeletal muscle development and plays an important role in myocyte proliferation (39, 63). Nerve growth factor has been shown to upregulate $K_V1.5$ and cause a decrease in AP decay time in myocytes cultured from 1- to 2-day old rat skeletal muscle (62). The lack of nerve growth factor in R6/2 skeletal muscle may lead to decreased $K_V1.5$ expression and muscle atrophy (3, 54). Also, $K_V1.5$ expression has been shown to be promoted by Sp-1, which in turn was shown to have increased activity in response to oxidative stress in myocytes (20). It is well established that mitochondrial dysfunction and oxidative stress play a pivotal role in HD pathology in both skeletal muscle and the CNS (59, 70). Because the expression of $K_V1.5$ and $K_V3.4$ is decreased in R6/2 skeletal muscle, it may be that Sp-1 can no longer respond to oxidative stress because it is bound to mutant huntingtin in HD.

Action Potential Recovery

We measured AP recovery for ~15 s following each AP train. The recovery followed two phases, a fast recovery occurring 125 ms after each AP train and a slow recovery occurring over the remaining time period. During the fast phase, the maximum repolarization recovered by ~30–50% in R6/2 and 9-AC/Ba^{2+} fibers but only 10% in WT fibers after the 40-Hz and 60-Hz trains. The rapid recovery of the maximum repolarization would increase the degree of $Na_V1.4$ relief from inactivation, which would explain the more rapid recovery in peak amplitude and maximum rate-of-rise we observed in R6/2 and 9-AC/Ba^{2+} fibers compared with WT.

The slow recovery phase of the AP maximum repolarization may be explained by the flux of K^+ and Cl^- from the t-tubules after sustained stimulation (1, 32). Our interpretation is that the reduction in ClC-1 and Kir currents limits the movement of K^+ into the t-tubules during trains in R6/2 and 9-AC/Ba^{2+} fibers. Thus, buildup of K^+ in t-tubules contributes more to the maximum repolarization of WT fibers than it does to R6/2 and 9-AC/Ba^{2+} fibers. This likely occurs because the mass movement of K^+ into the t-tubules must be accompanied by counter ions to maintain bulk electroneutrality, which is achieved with Cl^- movement through ClC-1 in WT muscle (9, 11, 13, 17, 33, 38, 43). Because ClC-1 currents are severely restricted in R6/2 and 9-AC/Ba^{2+} fibers, K^+ fluxes may be decreased. Overall, this suggests that ClC-1 and Kir dampen rapid voltage changes in WT fibers caused by subthreshold currents but facilitate the bulk movement of K^+ and Cl^-. This highlights a key role of Cl^- movement in WT muscle, which is consistent with work examining the role of ClC-1 in regulating muscle during normal activity (15, 48–50), and a recent study has described Cl^- movement with a four-electrode technique (26). In contrast to WT, R6/2 and 9-AC/Ba^{2+} fibers are more prone to rapid voltage changes caused by subthreshold currents but less susceptible to slow voltage changes caused by altered ion gradients.

Unlike the other AP parameters, there were no changes in the AP decay time during the fast recovery period in WT, R6/2, or 9-AC/Ba^{2+} fibers. Moreover, the 80% decay time of WT APs continued to prolong during the fast recovery period. The recovery of the 40% and 80% decay in R6/2 and 9-AC/Ba^{2+} fibers occurred with a time constant of 1–2 s, which is consistent with the reported recovery from inactivation for K_V, including $K_V3.4$ (e.g., 1.8-s time constant in dorsal root ganglion neurons) (53). Thus, it is likely that recovery from inactivation of the remaining $K_V1.5$ and $K_V3.4$ explains the exponential recovery phase recorded for R6/2 and 9-AC/Ba^{2+} fibers. In WT fibers, K^+ buildup in the t-tubules (1, 2, 21, 67, 69) and the prolonged recovery of the AP maximum repolarization may further delay the recovery from inactivation of $K_V1.5$ and $K_V3.4$.

It is worthwhile to comment on the strengths and limitations of this study. Experiments were conducted with fully mature muscle fibers on the day they were dissected from the mice, and the methods used were a direct extension of our previous voltage clamp studies of ClC-1 and Kir (44, 68). However, our acute block of ClC-1 and Kir to mimic disease conditions would not account for long-term compensatory changes in the R6/2 muscle. Another key consideration is the use of flexor digitorum brevis and interosseus fibers. Because of the small size of these muscle fibers, we were able control the intracellular as well as extracellular conditions. Our use of high intracellular EGTA blocked contractions even during 60-Hz trains. However, the EGTA may have inhibited Ca^{2+}-dependent signaling pathways. Indeed, several lines of evidence indicate that ClC-1 is regulated by signaling pathways that may be inhibited by EGTA (48–50, 60, 64). Future studies will be needed to extend this work to more physiological conditions, such as nondissociated muscle and different muscle groups with different fiber type compositions. Ultimately, the work will need to be extended to contractility studies and in vivo behavior measurements. Regarding Huntington's disease, additional studies will aim to corroborate these findings in R6/2 mice to additional disease models and to human patients. Overall, the high level of experimental control and ability to directly link to voltage clamp experiments makes the flexor digitorum brevis and interosseus fibers a very good starting point for mechanistic studies of mature wild-type and disease muscle.

Conclusion

Broadly, this study shows that APs in WT and disease muscle undergo significant and progressive changes in the rising and falling phases, peak, and baseline (maximum repolarization) during trains of activity. The dynamic nature of APs has implications for basic assessments of muscle function. For example, changes in electromyography (EMG) records are sometimes assumed to reflect changes in muscle function under the assumption that muscle APs are unchanging because of their all-or-none characteristics. However, it is likely that changes in EMG waveforms simply reflect changes in the APs of individual muscle fibers, such as the widening of the AP during trains, as shown in this study.

During trains, we found a substantial decrease in the AP maximum rate-of-rise, particularly in R6/2 fibers at high frequencies of stimulation. This was likely because the depolarizing shift in the maximum repolarization inactivated many $Na_V1.4$ channels. Despite the inactivation of $Na_V1.4$, the AP peak decreased by only a few millivolts. Our interpretation is that a corresponding inactivation of K_V channels during trains, as indicated by the widening of the APs, served to maintain the AP peak. In short, because of the reduced K^+ currents, less Na^+ current was needed to achieve a nearly normal AP peak. Eventually, the declining AP peak will cause muscle weakness once $Ca_V1.1$ is insufficiently activated. Weakness or fatigue is expected to occur sooner in R6/2 muscle than in WT because of the consistently reduced AP peak in R6/2 fibers. This work provides the foundation to determine the role of AP defects in R6/2 HD muscle dysfunction and to determine the ion channel regulatory events that modulate APs in WT and disease muscle.

ACKNOWLEDGMENTS

We thank Dr. William Romine for helpful discussion about the project and the Wright State University Biomedical Sciences PhD Program for their support of D.R.M.

GRANTS

This work was supported by NIH/National Institute of Neurological Disorders and Stroke Grant R15-NS-099850 (A.A.V.) and NIH/National Institute of Arthritis and Musculoskeletal and Skin Diseases Grant AR-074985 (M.M.R).

DISCLOSURES

No conflicts of interest, financial or otherwise, are declared by the authors.

AUTHOR CONTRIBUTIONS

D.R.M., A.J., M.B., H.R., M.M.R., and A.A.V. conceived and designed research; D.R.M., E.R., A.J., and A.A.V. performed experiments; D.R.M., E.R., A.J., M.B., H.R., and A.A.V. analyzed data; D.R.M., E.R., M.B., H.R., M.M.R., and A.A.V. interpreted results of experiments; D.R.M., A.J., H.R., and A.A.V. prepared figures; D.R.M., M.B., H.R., M.M.R., and A.A.V. drafted manuscript; D.R.M., E.R., M.B., H.R., M.M.R., and A.A.V. edited and revised manuscript; D.R.M., E.R., A.J., M.B., H.R., M.M.R., and A.A.V. approved final version of manuscript.

REFERENCES

1. **Adrian RH, Bryant SH.** On the repetitive discharge in myotonic muscle fibres. *J Physiol* 240: 505–515, 1974. doi:10.1113/jphysiol.1974.sp010620.
2. **Adrian RH, Marshall MW.** Action potentials reconstructed in normal and myotonic muscle fibres. *J Physiol* 258: 125–143, 1976. doi:10.1113/jphysiol.1976.sp011410.
3. **Alberch J, Pérez-Navarro E, Canals JM.** Neurotrophic factors in Huntington's disease. *Prog Brain Res* 146: 197–229, 2004. doi:10.1016/s0079-6123(03)46014-7.
4. **Allen DG, Lamb GD, Westerblad H.** Skeletal muscle fatigue: cellular mechanisms. *Physiol Rev* 88: 287–332, 2008. doi:10.1152/physrev.00015.2007.
5. **Ariano MA, Cepeda C, Calvert CR, Flores-Hernández J, Hernández-Echeagaray E, Klapstein GJ, Chandler SH, Aronin N, DiFiglia M, Levine MS.** Striatal potassium channel dysfunction in Huntington's disease transgenic mice. *J Neurophysiol* 93: 2565–2574, 2005. doi:10.1152/jn.00791.2004.
6. **Beam KG, Donaldson PL.** A quantitative study of potassium channel kinetics in rat skeletal muscle from 1 to 37 degrees C. *J Gen Physiol* 81: 485–512, 1983. doi:10.1085/jgp.81.4.485.
7. **Bradford J, Shin Y, Roberts M, Wang CE, Li J, Li S.** Expression of mutant huntingtin in mouse brain astrocytes causes age-dependent neurological symptoms. *Proc Natl Acad Sci USA* 106: 22480–22485, 2009. doi:10.1073/pnas.0911503106.
8. **Braubach P, Orynbayev M, Andronache Z, Hering T, Landwehrmeyer GB, Lindenberg KS, Melzer W.** Altered Ca^{2+} signaling in skeletal muscle fibers of the R6/2 mouse, a model of Huntington's disease. *J Gen Physiol* 144: 393–413, 2014. doi:10.1085/jgp.201411255.
9. **Bretag AH.** Muscle chloride channels. *Physiol Rev* 67: 618–724, 1987. doi:10.1152/physrev.1987.67.2.618.
10. **Busse ME, Hughes G, Wiles CM, Rosser AE.** Use of hand-held dynamometry in the evaluation of lower limb muscle strength in people with Huntington's disease. *J Neurol* 255: 1534–1540, 2008. doi:10.1007/s00415-008-0964-x.
11. **Cairns SP, Hing WA, Slack JR, Mills RG, Loiselle DS.** Different effects of raised [K+]o on membrane potential and contraction in mouse fast- and slow-twitch muscle. *Am J Physiol* 273: C598–C611, 1997. doi:10.1152/ajpcell.1997.273.2.C598.
12. **Catterall WA.** Voltage-gated sodium channels at 60: structure, function and pathophysiology. *J Physiol* 590: 2577–2589, 2012. doi:10.1113/jphysiol.2011.224204.
13. **Coonan JR, Lamb GD.** Effect of transverse-tubular chloride conductance on excitability in skinned skeletal muscle fibres of rat and toad. *J Physiol* 509: 551–564, 1998. doi:10.1111/j.1469-7793.1998.551bn.x.
14. **Cruickshank T, Reyes A, Peñailillo L, Thompson J, Ziman M.** Factors that contribute to balance and mobility impairments in individuals with Huntington's disease. *Basal Ganglia* 4: 67–70, 2014. doi:10.1016/j.baga.2014.04.002.
15. **de Paoli FV, Ørtenblad N, Pedersen TH, Jørgensen R, Nielsen OB.** Lactate per se improves the excitability of depolarized rat skeletal muscle by reducing the Cl^- conductance. *J Physiol* 588: 4785–4794, 2010. doi:10.1113/jphysiol.2010.196568.
16. **DiFranco M, Yu C, Quiñonez M, Vergara JL.** Inward rectifier potassium currents in mammalian skeletal muscle fibres. *J Physiol* 593: 1213–1238, 2015. doi:10.1113/jphysiol.2014.283648.
17. **Dulhunty AF.** Distribution of potassium and chloride permeability over the surface and T-tubule membranes of mammalian skeletal muscle. *J Membr Biol* 45: 293–310, 1979. doi:10.1007/BF01869290.
18. **Euler P, Friedrich B, Ziegler R, Kuhn A, Lindenberg KS, Weiller C, Zucker B.** Gene expression analysis on a single cell level in Purkinje cells of Huntington's disease transgenic mice. *Neurosci Lett* 517: 7–12, 2012. doi:10.1016/j.neulet.2012.03.080.
19. **Featherstone DE, Richmond JE, Ruben PC.** Interaction between fast and slow inactivation in Skm1 sodium channels. *Biophys J* 71: 3098–3109, 1996. doi:10.1016/S0006-3495(96)79504-8.
20. **Fountain SJ, Cheong A, Li J, Dondas NY, Zeng F, Wood IC, Beech DJ.** $K_V1.5$ potassium channel gene regulation by Sp1 transcription factor and oxidative stress. *Am J Physiol Heart Circ Physiol* 293: H2719–H2725, 2007. doi:10.1152/ajpheart.00637.2007.
21. **Fraser JA, Huang CL, Pedersen TH.** Relationships between resting conductances, excitability, and t-system ionic homeostasis in skeletal muscle. *J Gen Physiol* 138: 95–116, 2011. doi:10.1085/jgp.201110617.
22. **Friedrich O, Weber C, von Wegner F, Chamberlain JS, Fink RH.** Unloaded speed of shortening in voltage-clamped intact skeletal muscle fibers from wt, mdx, and transgenic minidystrophin mice using a novel high-speed acquisition system. *Biophys J* 94: 4751–4765, 2008. doi:10.1529/biophysj.107.126557.
23. **Goldin AL, Barchi RL, Caldwell JH, Hofmann F, Howe JR, Hunter JC, Kallen RG, Mandel G, Meisler MH, Netter YB, Noda M, Tamkun MM, Waxman SG, Wood JN, Catterall WA.** Nomenclature of voltage-gated sodium channels. *Neuron* 28: 365–368, 2000. doi:10.1016/S0896-6273(00)00116-1.
24. **González E, Messi ML, Zheng Z, Delbono O.** Insulin-like growth factor-1 prevents age-related decrease in specific force and intracellular Ca^{2+} in single intact muscle fibres from transgenic mice. *J Physiol* 552: 833–844, 2003. doi:10.1113/jphysiol.2003.048165.
25. **Hawash AA, Voss AA, Rich MM.** Inhibiting persistent inward sodium currents prevents myotonia. *Ann Neurol* 82: 385–395, 2017. doi:10.1002/ana.25017.
26. **Heiny JA, Cannon SC, DiFranco M.** A four-electrode method to study dynamics of ion activity and transport in skeletal muscle fibers. *J Gen Physiol* 151: 1146–1155, 2019. doi:10.1085/jgp.201912398.
27. **Hodgkin AL, Horowicz P.** The influence of potassium and chloride ions on the membrane potential of single muscle fibres. *J Physiol* 148: 127–160, 1959. doi:10.1113/jphysiol.1959.sp006278.

28. **Hodgkin AL, Huxley AF.** A quantitative description of membrane current and its application to conduction and excitation in nerve. *J Physiol* 117: 500–544, 1952. doi:10.1113/jphysiol.1952.sp004764.
29. **Hodgkin AL, Katz B.** The effect of sodium ions on the electrical activity of giant axon of the squid. *J Physiol* 108: 37–77, 1949. doi:10.1113/jphysiol.1949.sp004310.
30. **Holm S.** A simple sequentially rejective multiple test procedure. *Scand J Stat* 6: 65–70, 1979.
31. **Hutter OF, Noble D.** The chloride conductance of frog skeletal muscle. *J Physiol* 151: 89–102, 1960.
32. **Jack JJB, Noble D, Tsien RW.** *Electric Current Flow in Excitable Cells*. Oxford, UK: Clarendon Press, 1983.
33. **Jentsch TJ, Steinmeyer K, Schwarz G.** Primary structure of *Torpedo marmorata* chloride channel isolated by expression cloning in *Xenopus* oocytes. *Nature* 348: 510–514, 1990. doi:10.1038/348510a0.
34. **Jiang R, Diaz-Castro B, Looger LL, Khakh BS.** Dysfunctional calcium and glutamate signaling in striatal astrocytes from Huntington's Disease model mice. *J Neurosci* 36: 3453–3470, 2016. doi:10.1523/JNEUROSCI.3693-15.2016.
35. **Kenward MG, Roger JH.** Small sample inference for fixed effects from restricted maximum likelihood. *Biometrics* 53: 983–997, 1997. doi:10.2307/2533558.
36. **Khedraki A, Reed EJ, Romer SH, Wang Q, Romine W, Rich MM, Talmadge RJ, Voss AA.** Depressed synaptic transmission and reduced vesicle release sites in Huntington's disease neuromuscular junctions. *J Neurosci* 37: 8077–8091, 2017. doi:10.1523/JNEUROSCI.0313-17.2017.
37. **Klapstein GJ, Fisher RS, Zanjani H, Cepeda C, Jokel ES, Chesselet M-F, Levine MS.** Electrophysiological and morphological changes in striatal spiny neurons in R6/2 Huntington's disease transgenic mice. *J Neurophysiol* 86: 2667–2677, 2001. doi:10.1152/jn.2001.86.6.2667.
38. **Koch MC, Steinmeyer K, Lorenz C, Ricker K, Wolf F, Otto M, Zoll B, Lehmann-Horn F, Grzeschik KH, Jentsch TJ.** The skeletal muscle chloride channel in dominant and recessive human myotonia. *Science* 257: 797–800, 1992. doi:10.1126/science.1379744.
39. **Lesage F, Attali B, Lazdunski M, Barhanin J.** Developmental expression of voltage-sensitive K^+ channels in mouse skeletal muscle and C2C12 cells. *FEBS Lett* 310: 162–166, 1992. doi:10.1016/0014-5793(92)81320-L.
40. **Metzger S, Dupont C, Voss AA, Rich MM.** Central role of subthreshold currents in myotonia. *Ann Neurol* 87: 175–183, 2020. doi:10.1002/ana.25646.
41. **Mielcarek M.** Huntington's disease is a multi-system disorder. *Rare Dis* 3: e1058464, 2015. doi:10.1080/21675511.2015.1058464.
42. **Mielcarek M, Toczek M, Smeets CJLM, Franklin SA, Bondulich MK, Jolinon N, Muller T, Ahmed M, Dick JRT, Piotrowska I, Greensmith L, Smolenski RT, Bates GP.** HDAC4-myogenin axis as an important marker of HD-related skeletal muscle atrophy. *PLoS Genet* 11: e1005021, 2015. doi:10.1371/journal.pgen.1005021.
43. **Miller C.** ClC chloride channels viewed through a transporter lens. *Nature* 440: 484–489, 2006. doi:10.1038/nature04713.
44. **Miranda DR, Wong M, Romer SH, McKee C, Garza-Vasquez G, Medina AC, Bahn V, Steele AD, Talmadge RJ, Voss AA.** Progressive Cl^- channel defects reveal disrupted skeletal muscle maturation in R6/2 Huntington's mice. *J Gen Physiol* 149: 55–74, 2017. doi:10.1085/jgp.201611603.
45. **Oyama F, Miyazaki H, Sakamoto N, Becquet C, Machida Y, Kaneko K, Uchikawa C, Suzuki T, Kurosawa M, Ikeda T, Tamaoka A, Sakurai T, Nukina N.** Sodium channel β4 subunit: down-regulation and possible involvement in neuritic degeneration in Huntington's disease transgenic mice. *J Neurochem* 98: 518–529, 2006. doi:10.1111/j.1471-4159.2006.03893.x.
46. **Palade PT, Barchi RL.** Characteristics of the chloride conductance in muscle fibers of the rat diaphragm. *J Gen Physiol* 69: 325–342, 1977. doi:10.1085/jgp.69.3.325.
47. **Palade PT, Barchi RL.** On the inhibition of muscle membrane chloride conductance by aromatic carboxylic acids. *J Gen Physiol* 69: 879–896, 1977. doi:10.1085/jgp.69.6.879.
48. **Pedersen TH, de Paoli FV, Flatman JA, Nielsen OB.** Regulation of ClC-1 and KATP channels in action potential-firing fast-twitch muscle fibers. *J Gen Physiol* 134: 309–322, 2009 [Erratum in *J Gen Physiol* 134: 523, 2009]. doi:10.1085/jgp.200910290.
49. **Pedersen TH, Macdonald WA, de Paoli FV, Gurung IS, Nielsen OB.** Comparison of regulated passive membrane conductance in action potential-firing fast- and slow-twitch muscle. *J Gen Physiol* 134: 323–337, 2009 [Errata in *J Gen Physiol* 134: 525, 2009]. doi:10.1085/jgp.200910291.
50. **Pedersen TH, Riisager A, de Paoli FV, Chen TY, Nielsen OB.** Role of physiological ClC-1 Cl^- ion channel regulation for the excitability and function of working skeletal muscle. *J Gen Physiol* 147: 291–308, 2016. doi:10.1085/jgp.201611582.
51. **Quayle JM, McCarron JG, Brayden JE, Nelson MT.** Inward rectifier K^+ currents in smooth muscle cells from rat resistance-sized cerebral arteries. *Am J Physiol Cell Physiol* 265: C1363–C1370, 1993. doi:10.1152/ajpcell.1993.265.5.C1363.
52. **Ribchester RR, Thomson D, Wood NI, Hinks T, Gillingwater TH, Wishart TM, Court FA, Morton AJ.** Progressive abnormalities in skeletal muscle and neuromuscular junctions of transgenic mice expressing the Huntington's disease mutation. *Eur J Neurosci* 20: 3092–3114, 2004. doi:10.1111/j.1460-9568.2004.03783.x.
53. **Ritter DM, Ho C, O'Leary ME, Covarrubias M.** Modulation of Kv3.4 channel N-type inactivation by protein kinase C shapes the action potential in dorsal root ganglion neurons. *J Physiol* 590: 145–161, 2012. doi:10.1113/jphysiol.2011.218560.
54. **Ruberti F, Capsoni S, Comparini A, Di Daniel E, Franzot J, Gonfloni S, Rossi G, Berardi N, Cattaneo A.** Phenotypic knockout of nerve growth factor in adult transgenic mice reveals severe deficits in basal forebrain cholinergic neurons, cell death in the spleen, and skeletal muscle dystrophy. *J Neurosci* 20: 2589–2601, 2000. doi:10.1523/JNEUROSCI.20-07-02589.2000.
55. **Sassone J, Colciago C, Cislaghi G, Silani V, Ciammola A.** Huntington's disease: the current state of research with peripheral tissues. *Exp Neurol* 219: 385–397, 2009. doi:10.1016/j.expneurol.2009.05.012.
56. **Steinmeyer K, Klocke R, Ortland C, Gronemeier M, Jockusch H, Gründer S, Jentsch TJ.** Inactivation of muscle chloride channel by transposon insertion in myotonic mice. *Nature* 354: 304–308, 1991. doi:10.1038/354304a0.
57. **Steinmeyer K, Ortland C, Jentsch TJ.** Primary structure and functional expression of a developmentally regulated skeletal muscle chloride channel. *Nature* 354: 301–304, 1991. doi:10.1038/354301a0.
58. **Strand AD, Aragaki AK, Shaw D, Bird T, Holton J, Turner C, Tapscott SJ, Tabrizi SJ, Schapira AH, Kooperberg C, Olson JM.** Gene expression in Huntington's disease skeletal muscle: a potential biomarker. *Hum Mol Genet* 14: 1863–1876, 2005. doi:10.1093/hmg/ddi192.
59. **Tobore TO.** Towards a comprehensive understanding of the contributions of mitochondrial dysfunction and oxidative stress in the pathogenesis and pathophysiology of Huntington's disease. *J Neurosci Res* 97: 1455–1468, 2019. doi:10.1002/jnr.24492.
60. **Tricarico D, Conte Camerino D, Govoni S, Bryant SH.** Modulation of rat skeletal muscle chloride channels by activators and inhibitors of protein kinase C. *Pflugers Arch* 418: 500–503, 1991. doi:10.1007/BF00497778.
61. **van der Burg JMM, Björkqvist M, Brundin P.** Beyond the brain: widespread pathology in Huntington's disease. *Lancet Neurol* 8: 765–774, 2009. doi:10.1016/S1474-4422(09)70178-4.
62. **Vigdor-Alboim S, Rothman C, Braiman L, Bak A, Langzam L, Yosef O, Sterengarz BB, Nawrath H, Brodie C, Sampson SR.** Discoordinate regulation of different K channels in cultured rat skeletal muscle by nerve growth factor. *J Neurosci Res* 56: 275–283, 1999. doi:10.1002/(SICI)1097-4547(19990501)56:3<275:AID-JNR7>3.0.CO;2-R.
63. **Villalonga N, Martínez-Mármol R, Roura-Ferrer M, David M, Valenzuela C, Soler C, Felipe A.** Cell cycle-dependent expression of Kv1.5 is involved in myoblast proliferation. *Biochim Biophys Acta* 1783: 728–736, 2008. doi:10.1016/j.bbamcr.2008.01.001.
64. **Voss AA.** Extracellular ATP inhibits chloride channels in mature mammalian skeletal muscle by activating P2Y1 receptors. *J Physiol* 587: 5739–5752, 2009. doi:10.1113/jphysiol.2009.179275.
65. **Vullhorst D, Jockusch H, Bartsch JW.** The genomic basis of K(V)3.4 potassium channel mRNA diversity in mice. *Gene* 264: 29–35, 2001. doi:10.1016/S0378-1119(01)00327-4.
66. **Vullhorst D, Klocke R, Bartsch JW, Jockusch H.** Expression of the potassium channel KV3.4 in mouse skeletal muscle parallels fiber type maturation and depends on excitation pattern. *FEBS Lett* 421: 259–262, 1998. doi:10.1016/S0014-5793(97)01577-9.
67. **Wallinga W, Meijer SL, Alberink MJ, Vliek M, Wienk ED, Ypey DL.** Modelling action potentials and membrane currents of mammalian skeletal muscle fibres in coherence with potassium concentration changes in the

T-tubular system. *Eur Biophys J* 28: 317–329, 1999. doi:10.1007/s002490050214.

68. **Waters CW, Varuzhanyan G, Talmadge RJ, Voss AA.** Huntington disease skeletal muscle is hyperexcitable owing to chloride and potassium channel dysfunction. *Proc Natl Acad Sci USA* 110: 9160–9165, 2013. doi:10.1073/pnas.1220068110.
69. **Yensen C, Matar W, Renaud JM.** K^+-induced twitch potentiation is not due to longer action potential. *Am J Physiol Cell Physiol* 283: C169–C177, 2002. doi:10.1152/ajpcell.00549.2001.
70. **Zielonka D, Piotrowska I, Marcinkowski JT, Mielcarek M.** Skeletal muscle pathology in Huntington's disease. *Front Physiol* 5: 380, 2014. doi:10.3389/fphys.2014.00380.